response. It is possible that the most appropriate gating function for values of θ near 90° differs from the $\cos^4$ relation best suited for the full range of θ.

It is interesting to note that the January observations occurred near southern summer, and that the average interplanetary magnetic field is almost purely azimuthal at Saturn's distance from the Sun. As a result, the dominant component of the field was perpendicular to Saturn's magnetic moment. Solar wind control of Saturn's magnetosphere could be significantly different near the equinoxes, when Saturn's axial tilt results in a 64.5° angle between the dominant, azimuthal field component and Saturn's magnetic moment. This would be a manifestation of a well-documented phenomenon at Earth[18], but made more extreme owing to the alignment between Saturn's magnetic moment and spin axis.

Overall, the January Cassini and HST measurements indicate that Saturn's magnetosphere, although similar in some respects to those of the Earth and Jupiter, is not simply an intermediate case. It resembles Earth's magnetosphere in that its auroral dynamics are strongly driven by solar wind conditions. But it differs from Earth's interaction with the solar wind by virtue of an evidently weak influence of the direction of the interplanetary magnetic field. This may either be a characteristic of Saturn's magnetosphere, or be a result of differences between the solar wind at 10 AU and 1 AU (specifically, the weaker north–south component of the solar wind magnetic field). The latter possibility suggests that Saturn's magnetospheric response to the solar wind may be primarily driven by solar wind shocks, a process that is observed at the Earth[2] but generally overshadowed by the strong response of Earth's magnetosphere to the orientation of the interplanetary magnetic field. This apparent insensitivity to the magnetic field orientation and sensitivity to solar wind dynamic pressure and/or motional electric field make Saturn's magnetosphere resemble that of Jupiter more than that of Earth. In contrast to Jupiter, where the influence of the solar wind is weak and the aurorae are largely due to internal processes, the solar wind plays a controlling role in Saturn's auroral dynamics. □

Received 9 September; accepted 27 December 2004; doi:10.1038/nature03333.

1. Dungey, J. W. Interplanetary magnetic field and the auroral zone. *Phys. Rev. Lett.* **6,** 47–48 (1961).
2. Hill, T. W., Dessler, A. J. & Goertz, C. K. in *Physics of the Jovian Magnetosphere* (ed. Dessler, A. J.) 353–394 (Cambridge Univ. Press, Cambridge, 1983).
3. Clarke, J. T. *et al.* Morphological differences of Saturn's ultraviolet aurorae and those of Earth and Jupiter. *Nature* doi:10.1038/nature03331 (this issue).
4. Meurant, M., Gerard, J.-C., Blockx, C., Hubert, B. & Coumans, V. Propagation of electron and proton shock-induced aurora and the role of the interplanetary magnetic field and solar wind. *J. Geophys. Res.* **109,** A10210, doi:10.1029/2004JA010453 (2004).
5. Cowley, S. W. H. & Bunce, E. J. Origin of the main auroral oval in Jupiter's coupled magnetosphere-ionosphere system. *Planet. Space Sci.* **49,** 1067–1088 (2001).
6. Zarka, P. & Genova, F. Low frequency jovian emissions and solar wind magnetic sector structure. *Nature* **306,** 767–768 (1983).
7. Desch, M. D. & Barrow, C. H. Direct evidence for solar wind control of Jupiter's hectometric wavelength radio emission. *J. Geophys. Res.* **89,** 6819–6823 (1984).
8. Gurnett, D. A. *et al.* Control of Jupiter's radio emissions and aurorae by the solar wind. *Nature* **415,** 985–987 (2002).
9. Kivelson, M. G. & Southwood, D. J. First evidence of IMF control of Jovian magnetospheric boundary locations: Cassini and Galileo magnetic field measurements compared. *Planet. Space Sci.* **51,** 891–898 (2003).
10. Southwood, D. J. & Kivelson, M. G. A new perspective concerning the influence of the solar wind on the Jovian magnetosphere. *J. Geophys. Res.* **106,** 6123–6130 (2001).
11. Cowley, S. W. H. & Bunce, E. J. Modulation of Jupiter's main auroral oval emissions by solar wind induced expansions and compressions of the magnetosphere. *Planet. Space Sci.* **51,** 57–79 (2003).
12. Desch, M. D. Evidence for solar wind control of Saturn radio emission. *J. Geophys. Res.* **87,** 4549–4554 (1982).
13. Young, D. T. *et al.* Cassini plasma spectrometer investigation. *Space Sci. Rev.* (in the press).
14. Kurth, W. S. *et al.* An Earth-like correspondence between Saturn's auroral features and radio emission. *Nature* doi:10.1038/nature03334 (this issue).
15. Hanlon, P. G. *et al.* On the evolution of the solar wind between 1 and 5AU at the time of the Cassini-Jupiter flyby: multi spacecraft observations of ICMEs including the formation of a merged interaction region. *J. Geophys. Res.* **109,** A09S03, doi:10.1029/2003JA010112 (2004).
16. Tóth, G. General code for modeling MHD flows on parallel computers: Versatile advection code. *Astrophys. Lett. Commun.* **34,** 245–250 (1996).
17. Akasofu, S.-I. The solar wind-magnetosphere energy coupling and magnetospheric disturbances. *Planet. Space Sci.* **28,** 495–509 (1980).
18. Russell, C. T. & McPherron, R. L. Semiannual variation of geomagnetic activity. *J. Geophys. Res.* **78,** 92–108 (1973).

Acknowledgements F.J.C., B.L.B., J.T.S. and D.T.Y. were supported by NASA through a Jet Propulsion Laboratory contract with SWRI; D.G.M., K.C.H. and W.S.K. were supported through other NASA/JPL contracts; P.G.H. was supported by a PPARC-UK quota studentship; and J.C.G. and D.G. were supported by the Belgian Foundation for Scientific Research (FNRS) and the PRODEX program of the ESA. This work is based on observations with the NASA/ESA Hubble Space Telescope, obtained at the Space Telescope Science Institute, which is operated by the AURA, Inc., for NASA.

Competing interests statement The authors declare that they have no competing financial interests.

Correspondence and requests for materials should be addressed to F.J.C. (fcrary@swri.edu).

An Earth-like correspondence between Saturn's auroral features and radio emission

W. S. Kurth[1], D. A. Gurnett[1], J. T. Clarke[2], P. Zarka[3], M. D. Desch[4], M. L. Kaiser[4], B. Cecconi[1], A. Lecacheux[3], W. M. Farrell[4], P. Galopeau[5], J.-C. Gérard[6], D. Grodent[6], R. Prangé[3], M. K. Dougherty[7] & F. J. Crary[8]

[1]*Department of Physics and Astronomy, The University of Iowa, Iowa City, Iowa 52242, USA*
[2]*Boston University, 725 Commonwealth Avenue, Boston, Massachusetts 02215, USA*
[3]*Space Research Department, Observatoire de Paris, 92195 Meudon, France*
[4]*NASA/Goddard Space Flight Center, Greenbelt, Maryland 20771, USA*
[5]*CETP/UVSQ, 78140 Velizy, France*
[6]*LPAP, Université de Liège, allée du 6 aout, 17, B-4000 - Liège, Belgium*
[7]*Blackett Laboratory, Imperial College of Science and Technology, London SW7 2BZ, UK*
[8]*Southwest Research Institute, Culebra Road, San Antonio, Texas 78288, USA*

Saturn is a source of intense kilometre-wavelength radio emissions that are believed to be associated with its polar aurorae[1,2], and which provide an important remote diagnostic of its magnetospheric activity. Previous observations implied that the radio emission originated in the polar regions, and indicated a strong correlation with solar wind dynamic pressure[1,3–7]. The radio source also appeared to be fixed near local noon and at the latitude of the ultraviolet aurora[1,2]. There have, however, been no observations relating the radio emissions to detailed auroral structures. Here we report measurements of the radio emissions, which, along with high-resolution images of Saturn's ultraviolet auroral emissions[8], suggest that although there are differences in the global morphology of the aurorae, Saturn's radio emissions exhibit an Earth-like correspondence between bright auroral features and the radio emissions. This demonstrates the universality of the mechanism that results in emissions near the electron cyclotron frequency narrowly beamed at large angles to the magnetic field[9,10].

The first studies of Saturn's primary radio emission (Saturn kilometric radiation, SKR) were by the Voyager spacecraft in the early 1980s[1,3]. This emission had some features that were more like those of Earth than of Jupiter: the SKR source appears to be fixed in local time, favouring a region near local late morning or noon, but varying with source latitude[2]. It is also strongly correlated with solar wind parameters, such as the dynamic pressure[7]. However, the SKR also has some features that are more like those of Jupiter than of Earth: it was found to be strongly modulated by planetary rotation, despite the fact that models of Saturn's magnetic field are axisymmetric[11]. This has suggested an as-yet-unobserved 'active sector' or possible 'magnetic anomaly' rotating with the planet[12,13].

The measurements shown here are primarily from the radio

and plasma wave science instrument on Cassini[14] and the Space Telescope Imaging Spectrograph (STIS) on the Hubble Space Telescope (HST)[8]. Cassini continuously monitors the intensity and polarization of SKR (typically observed between ~20 and 800 kHz). During the month of January 2004, the observed SKR was almost entirely left-hand circularly polarized, consistent with emissions from Saturn's southern hemisphere. This is largely due to the fact that Cassini was at a saturnian latitude of about −16°. We use this dominance of left-hand circularly polarized emission to derive the total hemispherical integrated radio flux at Cassini by using only this polarization to eliminate contributions from solar type III bursts and a few other low-frequency emissions. Similarly, the ultraviolet observations are restricted to the southern hemisphere by the viewing geometry from Earth. In Fig. 1 we compare the integrated power per unit solid angle with the power input to the aurora. The plot in Fig. 1a shows a general correspondence between the auroral input power and SKR. Given some Voyager estimates of the SKR rotationally averaged solid angle of 2π sr (ref. 6), we obtain emission efficiencies of about 0.5%. This is comparable to the efficiency of generating terrestrial kilometric radiation[15] (~1%).

The plot of the auroral input power and SKR emitted power, shown in Fig. 1c, provides a more quantitative analysis of the relation between these two parameters. The linear fit to these data gives a positive correlation coefficient, r, of 0.87. However, without the two large-amplitude points obtained on 26 and 28 January, the remaining points are not correlated. Perhaps one reason for this is the large disparity in the measurement duration for the two parameters; 10.67 h for SKR and about 20 min for the ultraviolet intensity. On the other hand, the two highest-amplitude points from the HST observations have the largest signal-to-noise ratio and, hence, are the most reliable. During the period encompassing the 26 and 28 January images, Saturn was under the influence of a corotating interaction region with high field amplitudes and increased solar wind dynamic pressure[16] (Fig. 1b).

A five-orbit sequence of HST observations acquired on 8 January 2004 is useful in understanding in greater detail the relation between the ultraviolet emissions and, in this case, relatively weak SKR emissions. The first image (Fig. 2, image (1) in the top row) shows that even though there is a relatively bright aurora near dawn, there is very little corresponding radio emission (Fig. 2, bottom panel). The next three images, (2) to (4) in Fig. 2, show the bright spot moving to increasing local times and latitudes while the radio emission spectrum intensifies and expands to lower frequencies. The last image (5) shows a weaker auroral emission that has moved off to the local afternoon just near the end of the SKR event. The ultraviolet power during this series of observations varies by more than a factor of three.

As Cassini is nearly fixed in position with respect to Saturn during this time, we can explore the relationship between the bright auroral features, which appear to be rotating at about 30–75% of corotation[8] with the planet, and the observed SKR, under the assumption that the SKR source, like terrestrial kilometric radiation, is tied to bright auroral features[15,17,18]. Using the Z3 model of Saturn's magnetic field[11], we can determine the geometry of magnetic field lines connected to the centroids of three bright auroral 'spots' (A, B, C) seen in each of the five ultraviolet images in Fig. 2. The altitude of the source is where the emission frequency equals the electron cyclotron frequency, f, given by $f = 28|B|$, where

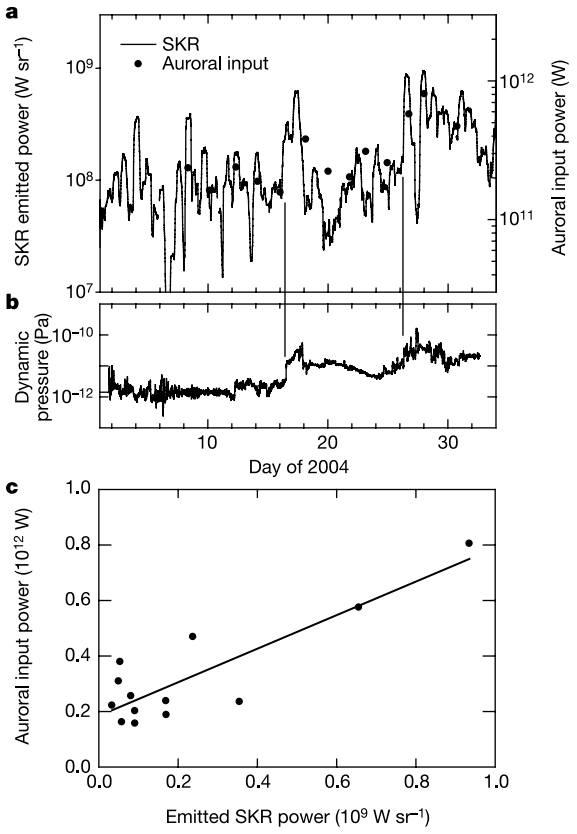

Figure 1 Correlations between auroral input power and emitted SKR power. **a**, Time-averaged power emitted as SKR as a function of time, overplotted with the estimated auroral input power based on the ultraviolet aurora integrated intensity. The radio power is a sliding 10 h 40 min (Saturn's approximate rotational period) average, using the left-hand circularly polarized component of the wave spectrum integrated between 10 kHz and 1 MHz. The rotational average is used because Voyager observations indicated that for short averaging intervals of the SKR power (less than several hours) there is no correlation between intensities observed by two widely spaced observers[5]. The auroral input power is estimated from the integrated ultraviolet intensity over the auroral region assuming electron precipitation[8]. **b**, Solar wind dynamic pressure determined from Cassini measurements of the solar wind density and speed, and propagated to Saturn with a simple radial magnetohydrodynamic model[16]. **c**, Plot comparing the auroral input power and emitted radio power.

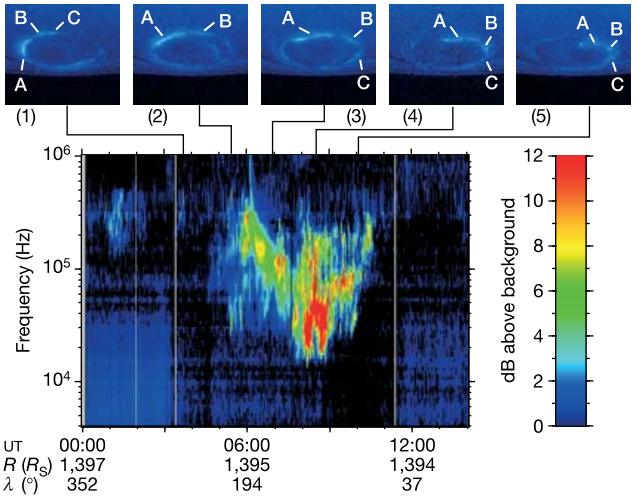

Figure 2 Detailed SKR observations from 8 January and the associated ultraviolet images. Top, five images covering about 70% of a Saturn rotation. Bottom, spectrogram displaying the intensity of radio waves (using the colour bar at the right) as a function of frequency (ordinate) and time (abscissa). At the bottom, R refers to the radial distance from Saturn in units of Saturn radii (R_S), and λ is longitude. The images[8] are obtained by the STIS instrument on the Hubble Space Telescope with the image brightness scaled to the observed intensity of ultraviolet emissions. Lines relate each image to the respective time on the spectrogram. The letters A, B and C indicate the centroid of bright spots referred to in Fig. 3.

f is in Hz and B (the magnetic field strength) is in nT. Without anticipating the beaming properties of the emission, we can determine, from purely geometric considerations, the emission angle with respect to the magnetic field for the radio source to be visible from Cassini at each frequency and for each of the images. The resulting acceptable combinations of beaming angles and frequencies are shown as thin lines in Fig. 3 for each image (1 to 5). Panels a, b and c show the respective results for spots labelled A, B and C in Fig. 2. The observed frequency ranges are plotted with thick lines. Beaming angles less than 90° in the southern hemisphere imply propagation towards the planet and increasing field strengths. As the extraordinary mode cannot propagate where $f < f_{ce}$ (f_{ce} is the electron cyclotron frequency), these solutions are unphysical. A source on field lines threading spots B or C cannot account for all of the observed emission observed in the five images; but a source associated with bright spot A can. Carrying this analysis further, it is possible to consider all the possible sources connected to spot A, for each image. We find that all of the observed emission can be explained by sources on field lines in the vicinity of spot A using only a narrow range of beaming angles, 110–125°. Hence it is possible to associate SKR with bright aurorae assuming relatively narrow emission cones.

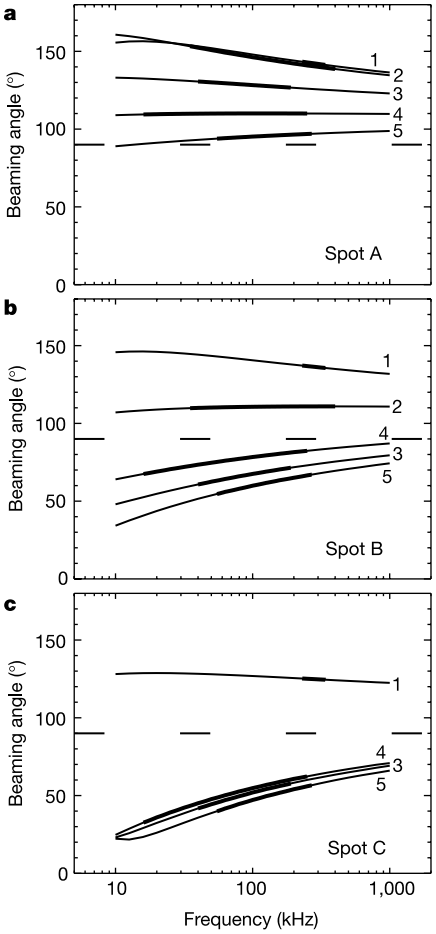

Figure 3 Beaming angles required to illuminate Cassini from radio sources associated with bright spots identified in Fig. 2. **a**, For the bright spot identified with an A in the images in Fig. 2; the thin lines indicate the beaming angle required for a radio wave to propagate from a source threading the centre of the bright spot labelled A to Cassini as a function of frequency. This construction is made assuming the emission frequency is at the electron cyclotron frequency and using the Z3 magnetic field model for Saturn[11]. The thick lines represent the range of frequencies actually observed at Cassini. The numbers refer to the five images at the top of Fig. 2. **b**, Similar to **a** but the geometry is for sources on a field line threading the bright spot labelled B in Fig. 2. **c**, Similar to **a** and **b** but for the bright spot identified with a C. The identification of this particular feature from one image to the next is less clear than for the others. Note that beaming angles greater than 90° (indicated by the dashed line) are directed away from Saturn and away from stronger field regions. Beaming angles less than 90° are directed downward towards the planet in order to intersect Cassini. The downward propagation, however, is forbidden by the presence of Saturn and the stronger magnetic fields near it; hence, these waves cannot reach Cassini.

Cassini does not observe the radio emissions for the entire frequency range all of the time. This is because the cyclotron maser instability produces many fluctuating, localized sources emitting in very narrow beams; localized and probably time variable differences between the Z3 model and the actual field also affect the visibility of the emissions. It is clear that the correlation between the ultraviolet and SKR power is limited, as HST can observe the entire auroral oval but the radio emissions are not always beamed in the direction of Cassini. Nevertheless, Fig. 3 demonstrates that SKR can be tied to bright aurorae, as is the case at Earth[15,17,18]. The thick lines in Fig. 3 for angles >90° may be interpreted as an ensemble average of emission extending in altitude from field lines threading the vicinity of the bright auroral spot A to account for the range in frequencies observed.

As spot A rotates through a limited range of local times during the sequence of images obtained on 8 January[8], and the local time range is generally consistent with that obtained for the SKR source region from Voyager observations, we now have sufficient information to clarify one of the conclusions based on Voyager observations—that the source is fixed in local time. We can now say that the source could, indeed, move as the bright spots are seen to move, but within a limited range of local times.

There is additional evidence that beaming is important for the detection of SKR. The large dip in SKR power seen on day 27 in Fig. 1a corresponds to a 'missing' SKR event; the usual modulation of SKR seems to skip a rotation on 27 January. However, the Unified Radio and Plasma Wave experiment[19] on the Ulysses[20] spacecraft, which is at slightly lower saturnian latitudes than Cassini, does see SKR during the expected time frame. During this time period, Saturn is under the influence of higher solar wind dynamic pressure associated with a corotating interaction region in the solar wind[16]. We believe that the higher solar wind dynamic pressure at this time distorts the field and moves the SKR beam away from Cassini. This evidence, although anecdotal, confirms that beaming must be considered in any detailed comparison of auroral brightness and SKR.

The bright aurora observed on 26 and 28 January[8] shows poleward expansion and is accompanied by intense SKR that spreads to lower frequencies. The total SKR power is a function of bandwidth, with larger fluxes seen with broader bandwidths. Clarke *et al.*[8] show that the auroral latitude and auroral power are correlated. At Earth, expansion of kilometric radiation to low frequencies is correlated with higher fluxes of auroral bremsstrahlung X-rays[21], so the association between the increase of the SKR bandwidth and intense aurora is a similarity between Earth and Saturn. Such a correlation between increased precipitation and expansion of SKR to lower frequencies is probably a result of the Knight relationship[22]; increased auroral currents require an increase in the upper altitude limit of the auroral acceleration region[23]. Consequently, the SKR source region probably expands to higher altitudes, where f_{ce} is lower. It is also likely that beaming plays a role in this frequency variation, given the poleward expansion of the aurora and that significant distortions in the magnetic field are possible as interplanetary shocks, varying interplanetary field orientations and solar wind dynamic pressure variations interact with the magnetosphere. □

Received 13 August; accepted 4 December 2004; doi:10.1038/nature03334.

1. Kaiser, M. L. *et al.* in *Saturn* (eds Gehrels, T. & Matthews, M. S.) 378–415 (Univ. Arizona Press, Tucson, 1984).

2. Galopeau, P. H. M., Zarka, P. & Le Quéau, D. Source location of Saturn's kilometric radiation: The Kelvin-Helmholtz instability hypothesis. *J. Geophys. Res.* **100,** 26397–26410 (1995).
3. Warwick, J. W. *et al.* Planetary radio astronomy observations from Voyager 1 near Saturn. *Science* **212,** 239–243 (1981).
4. Galopeau, P. H. M. & Lecacheux, A. Variations in Saturn's radio rotation period measured at kilometer wavelengths. *J. Geophys. Res.* **105,** 13089–13101 (2000).
5. Zarka, P. in *Planetary Radio Emissions II* (eds Rucker, H. O., Bauer, S. J. & Pedersen, B. M.) 327–342 (Austrian Acad. Sci. Press, Vienna, 1988).
6. Zarka, P. Auroral radio emissions at the outer planets: Observations and theories. *J. Geophys. Res.* **103,** 20159–20194 (1998).
7. Desch, M. D. Evidence for solar wind control of Saturn radio emission. *J. Geophys. Res.* **87,** 4549–4554 (1982).
8. Clarke, J. T. *et al.* Morphological differences of Saturn's ultraviolet aurorae and those of Earth and Jupiter. *Nature* doi:10.1038/nature03331 (this issue).
9. Wu, C. S. & Lee, L. C. A theory of terrestrial kilometric radiation. *Astrophys. J.* **230,** 621–626 (1979).
10. Galopeau, P., Zarka, P. & Le Quéau, D. Theoretical model of Saturn's kilometric radiation spectrum. *J. Geophys. Res.* **94,** 8739–8755 (1989).
11. Connerney, J. E. P., Ness, N. F. & Acuña, M. H. Zonal harmonic model of Saturn's magnetic field from Voyager 1 and 2 observations. *Nature* **298,** 44–46 (1982).
12. Galopeau, P., Ortega-Molina, A. & Zarka, P. Evidence of Saturn's magnetic field anomaly from SKR high-frequency limit. *J. Geophys. Res.* **96,** 14129–14140 (1991).
13. Galopeau, P. & Zarka, P. Reply to the comment by J. E. P. Connerney and M. D. Desch on "Evidence of Saturn's magnetic field anomaly from SKR high-frequency limit". *J. Geophys. Res.* **97,** 12291–12297 (1992).
14. Gurnett, D. A. *et al.* The Cassini radio and plasma wave science investigation. *Space Sci. Rev.* (in the press).
15. Gurnett, D. A. The Earth as a radio source: Terrestrial kilometric radiation. *J. Geophys. Res.* **79,** 4227–4238 (1974).
16. Crary, F. J. *et al.* Solar wind dynamic pressure and electric field as the main factors controlling Saturn's aurorae. *Nature* doi:10.1038/nature03333 (this issue).
17. Huff, R. L., Calvert, W., Craven, J. D., Frank, L. A. & Gurnett, D. A. Mapping of auroral kilometric radiation sources to the aurora. *J. Geophys. Res.* **93,** 11445–11454 (1988).
18. de Feraudy, H., Bahnsen, A. & Jespersen, M. in *Planetary Radio Emissions II* (eds Rucker, H. O., Bauer, S. J. & Pedersen, B. M.) 41–60 (Austrian Acad. Sci. Press, Vienna, 1988).
19. Stone, R. G. *et al.* The unified radio and plasma wave investigation. *Astron. Astrophys. Suppl. Ser.* **92,** 291–316 (1992).
20. Wenzel, K. P., Marsden, R. G., Page, D. E. & Smith, E. J. The Ulysses mission. *Astron. Astrophys. Suppl. Ser.* **92,** 207–219 (1992).
21. Imhof, W. L. *et al.* The dependence of AKR production on the intensity and energy spectra of auroral bremsstrahlung. *J. Geophys. Res.* **108,** doi:10.1029/2002JA009274 (2003).
22. Knight, S. Parallel electric fields. *Planet. Space Sci.* **21,** 741–750 (1973).
23. Cowley, S. W. H. & Bunce, E. J. Origin of the main auroral oval in Jupiter's coupled magnetosphere-ionosphere system. *Planet. Space Sci.* **49,** 1067–1088 (2001).

Acknowledgements This research was supported by NASA through contracts with the Jet Propulsion Laboratory. J.-C.G. and D.G. are supported by the Belgian Fund for Scientific Research (FNRS) and partly funded by the PRODEX programme of the European Space Agency. This work is based on observations with the NASA/ESA Hubble Space Telescope, obtained at the Space Telescope Science Institute, which is operated by AURA, Inc., for NASA.

Competing interests statement The authors declare that they have no competing financial interests.

Correspondence and requests for materials should be addressed to W.S.K. (william-kurth@uiowa.edu).

A continuous-wave Raman silicon laser

Haisheng Rong[1], Richard Jones[1], Ansheng Liu[1], Oded Cohen[2], Dani Hak[2], Alexander Fang[1] & Mario Paniccia[1]

[1]*Intel Corporation, 2200 Mission College Blvd, CHP3-109, Santa Clara, California 95054, USA*
[2]*Intel Corporation, SBI Park Har Hotzvim, Jerusalem, 91031, Israel*

Achieving optical gain and/or lasing in silicon has been one of the most challenging goals in silicon-based photonics[1–3] because bulk silicon is an indirect bandgap semiconductor and therefore has a very low light emission efficiency. Recently, stimulated Raman scattering has been used to demonstrate light amplification and lasing in silicon[4–9]. However, because of the nonlinear optical loss associated with two-photon absorption (TPA)-induced free carrier absorption (FCA)[10–12], until now lasing has been limited to pulsed operation[8,9]. Here we demonstrate a continuous-wave silicon Raman laser. Specifically, we show that TPA-induced FCA in silicon can be significantly reduced by introducing a reverse-biased p-i-n diode embedded in a silicon waveguide. The laser cavity is formed by coating the facets of the silicon waveguide with multilayer dielectric films. We have demonstrated stable single mode laser output with side-mode suppression of over 55 dB and linewidth of less than 80 MHz. The lasing threshold depends on the p-i-n reverse bias voltage and the laser wavelength can be tuned by adjusting the wavelength of the pump laser. The demonstration of a continuous-wave silicon laser represents a significant milestone for silicon-based optoelectronic devices.

The continuous-wave (c.w.) silicon Raman laser is constructed from a low-loss silicon-on-insulator (SOI) rib waveguide whose facets are coated with multilayer dielectric films. The front facet coating is dichroic, having a reflectivity (R_f) of ~71% for the Raman/Stokes wavelength of 1,686 nm and ~24% for the pump wavelength of 1,550 nm. The back facet has a broadband high-reflectivity coating (R_b) of ~90% for both pump and Raman wavelengths (Fig. 1a). These waveguide facet reflectivities were determined using a Fabry–Pérot resonance technique[2].

The silicon rib waveguide is fabricated on the (100) surface of an undoped SOI substrate using standard photolithographic patterning and reactive ion etching techniques. We designed the waveguide dimensions with the goal of obtaining a small cross-section for minimizing the required optical power to achieve the lasing threshold, but not so small as to cause high transmission loss. A cross-section scanning electron microscope image of a typical p-i-n waveguide is shown in Fig. 1b. The rib waveguide dimensions are: rib width (W) ~1.5 μm; height (H) ~1.55 μm; and etch depth (h) ~0.7 μm. The effective core area[13] of the waveguide is calculated to

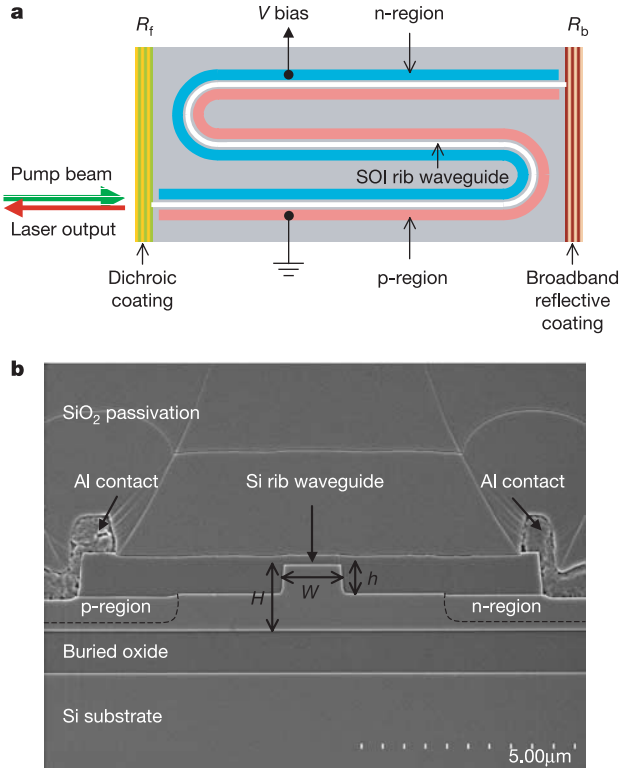

Figure 1 Silicon waveguide used in the Raman laser experiment. **a**, Schematic layout of the silicon waveguide laser cavity with optical coatings applied to the facets and a p-i-n structure along the waveguide. **b**, Scanning electron microscope cross-section image of a silicon rib waveguide with a p-i-n diode structure.